

**High resolution infrared study of the $2\nu_9$ and ν_4 bands of $10\text{BF}_2\text{OH}$ and $11\text{BF}_2\text{OH}$:
Evidence of large amplitude effects for the OH- torsion -
bending modes in the 9^2 and 4^1 and excited states.**

Journal:	<i>Molecular Physics</i>
Manuscript ID:	TMPH-2007-0069.R1
Manuscript Type:	Full Paper
Date Submitted by the Author:	13-Apr-2007
Complete List of Authors:	Perrin, Agnes; CNRS, Universite Paris 12 BERTSEVA, Elena; LISA Flaud, J. M.; LISA, Uni. Paris12 Collet, david; FBC Universitat Buerger, Hans; FBC Universitat masiello, tony; PNNL Blake, Thomas; PNNL
Keywords:	large amplitude torsion, large amplitude bending, infrared, staggering, axis switching effects



16/04/2007

1

1
2
3 **High resolution infrared study of the $2\nu_9$ and ν_4 bands of $^{10}\text{BF}_2\text{OH}$ and $^{11}\text{BF}_2\text{OH}$:**
4 **Evidence of large amplitude effects for the OH- torsion -bending modes in the**
5 **9^2 and 4^1 and excited states.**
6
7
8
9

10 A.PERRIN[§](1), E.BERTSEVA[¶](1), J.-M.FLAUD (1)

11 D.COLLET(2), H. BÜRGER(2)

12 T. MASIELLO(3), and T. A. BLAKE(3),
13
14
15
16

17 (1) Laboratoire Interuniversitaire des Systèmes Atmosphériques (LISA),
18 CNRS/Universités Paris 12 et Paris 7, 61 av. du Général de Gaulle, 94010 Créteil
19 Cedex, France
20
21
22

23 (2) Anorganische Chemie, FBC, Universität, D-42097 Wuppertal, Germany
24
25
26

27 (3) Pacific Northwest National Laboratory (PNNL), P. O. Box 999, Mail Stop K8-88,
28 Richland, WA 99352, USA
29
30
31
32

33 No. of figures: 7

34 No. of tables: 10

35 [§]Corresponding author: A.Perrin, Laboratoire Interuniversitaire des Systèmes
36 Atmosphériques, (LISA), CNRS/Universités Paris 12 et Paris 7, 61 av. du Général de
37 Gaulle, 94010 Créteil Cedex, France,
38 Tel. 33(0)14517 6557, Fax. 33(0)145171564, Email: perrin@lisa.univ-paris12.fr
39
40
41
42
43
44

45 [¶]Present address : E.Bertseva, Institut de Physique de la Matière Complexe, Ecole
46 Polytechnique Fédérale de Lausanne (EPFL), CH-1015 Lausanne, Switzerland
47
48
49
50
51
52
53
54
55
56
57
58
59
60

16/04/2007

2

Abstract

High resolution ($2\text{-}3 \times 10^{-3} \text{cm}^{-1}$) Fourier transform infrared spectra of gas phase ^{10}B and ^{11}B enriched and natural samples of BF_2OH (difluoroboric acid) were recorded at Wuppertal and Richland. Starting from the results of previous studies [A.Perrin, M.Carvajal-Zaera, Z.Dutkiewicz, J.-M.Flaud, D.Collet, H.Bürger, J.Demaison, F.Willaert, H.Mäder, and N.W.Larsen, *Mol. Phys.* **102**, 1641 (2004); J. Breidung, J. Demaison, J.-F. D'Eu, L. Margulès, D. Collet, E.B. Mkadmi, A. Perrin and W. Thiel, *J. Mol. Spectrosc.* **228**, 7, (2004)], it was possible to perform the first rovibrational analysis of the $2\nu_9$ (first overtone of ν_9 , the OH torsion) and ν_4 (BOH bending) bands located at about 1043.9 and 961.7 cm^{-1} and 1042.9 and 961.5 cm^{-1} for the $^{10}\text{BF}_2\text{OH}$ and $^{11}\text{BF}_2\text{OH}$ isotopic species respectively. Numerous "classical" perturbations were observed in the analysis of the $2\nu_9$ and ν_4 bands. The energy levels of the 9^2 bright state are indeed involved in a B-type Coriolis resonance with those of the $6^1 9^1$ dark state. The 4^1 levels are perturbed by a B-type Coriolis resonance and by an anharmonic resonance with the levels of the $7^1 9^1$ and the $6^1 7^1$ dark states respectively. In addition large amplitude effects were observed for the $2\nu_9$ and also, more surprisingly, the ν_4 bands. This results in splittings of the energy levels of about 0.005 and 0.0035 cm^{-1} for the 9^2 and 4^1 states respectively which are easily observable in the P and R branches for both bands. The theoretical model used to reproduce the experimental levels accounts for the classical vibration-rotation resonances. Also the large amplitude torsional (or bending) effects are accounted for within the frame of the IAM (Internal Axis Method) -like approach. The Coriolis resonances between the two torsional (or bending) substates are taken into account by $\{J_x, J_z\}$ non orthorhombic terms in the v -diagonal blocks. This means that the z -quantification axis deviates from the a inertial axis by an axis switching effect of $\sim 35^\circ$ for the $\{9^2, 6^1 9^1\}$ system and of $\sim 16.6^\circ$ for the $\{4^1, 7^1 9^1, 6^1 7^1\}$ system of interacting vibrational states. The calculation of the relative line intensities for the $2\nu_9$ and ν_4 bands accounts for these axis switching effects as well as for the intensity alternation which is due to the nuclear spin statistical weights since the OH large amplitude torsion and/or bending motion results indeed in an exchange of the two fluorine nuclei.

16/04/2007

3

Keywords: large amplitude torsion, large amplitude bending mode, splitting, infrared, staggering

1. Introduction

BF₂OH, difluoroboric acid, is a reactive intermediate in the hydrolysis of BF₃. It is a planar asymmetric rotor which is isovalent with HONO₂ (nitric acid). The microwave spectrum was first measured by Takeo and Curl [1] and later on by Vormann and Dreizler [2]. These investigations were extended recently since at Lille new millimeterwave spectra of the ¹⁰BF₂OH and ¹¹BF₂OH isotopic species¹ in their ground vibrational state were measured [3]. As a result, accurate ground state rotational and centrifugal distortion constants were determined for these isotopic species. Also, new and accurate *ab initio* structure and anharmonic force fields have been calculated leading to the determination of an accurate equilibrium structure for BF₂OH [3]. Figure 1 gives a picture of the BF₂OH molecule together with some of the conventions which are used in this study.

As far as infrared data are concerned, Jacox *et al.* [4] observed the matrix infrared (IR) spectra of eight isotopologues. The assignments were supported by *ab initio* calculations of the structure and the harmonic force field. The first high resolution IR spectrum of BF₂OH in the gas phase was observed by Collet *et al.* [5] using a Fourier transform (FT) spectrometer at Wuppertal. In this way the first analyses of the ν_8 and ν_9 fundamental bands of 11B located at 684.160 and 522.870 cm⁻¹, respectively were performed. Later on, the ν_5 , ν_8 , ν_9 and $\nu_8+\nu_9$ bands of 10B, and ν_7 , ν_5 , and $\nu_8+\nu_9$ bands of 11B were analysed for the first time up to very high rotational quantum numbers [6]. It was observed that the ν_5 , ν_8 , ν_9 and $\nu_8+\nu_9$ bands of 10B and the $\nu_8+\nu_9$ band of 11B are not significantly affected by perturbations. For the ν_5 and ν_7 bands of 11B C-type Coriolis interactions coupling the 5¹ and 7¹ energy levels with those of

¹ For the ¹⁰BF₂OH and ¹¹BF₂OH isotopic species we will use henceforth in the text the abbreviated notation 10B and 11B respectively. Properties and values, X, given both for 10B and 11B are quoted ¹⁰X(¹¹X), with values for 11B given in parentheses. For conciseness, properties Y referring both to the 9² and 4¹ polyads of interacting systems are labelled Y9²/Y4¹ using a slash throughout the present work.

16/04/2007

4

1
2
3 the 7^2 and 6^1 dark states respectively had to be accounted for in the calculations.
4
5 Table 1 lists the infrared bands of BF_2OH .
6
7

8
9 The present study presents the first analysis of the $2\nu_9$ and ν_4 bands both for 10B and
10 11B. These bands which correspond respectively to the first overtone of the OH
11 torsional mode (ν_9) and the OH bending mode (ν_4) are analysed together in the
12 present study because the levels of the 9^2 and 4^1 upper states are both split due to
13 large amplitude motions of the OH bond. The line splittings, of about 0.005 and
14 0.0035 cm^{-1} in $2\nu_9$ and ν_4 respectively, are easily observed in the whole range of the
15 IR spectra. It should be mentioned that on the contrary no such splittings were
16 detected during the infrared analyses of the ν_5 , ν_7 , ν_8 , ν_9 and $\nu_8+\nu_9$ bands [6].
17
18
19
20
21
22
23

24
25 It is interesting, for theoretical reasons, to compare difluoroboric acid, ($\text{F} \text{---} \text{B} \text{---} \text{O} \text{---} \text{H}$)
26
27
28 to one of its isoelectronic molecules, nitric acid ($\text{O} \text{---} \text{N} \text{---} \text{O} \text{---} \text{H}$). For HNO_3 , the ν_9
29 mode (torsion of the OH bond relative to the NO_2 moiety) is a large amplitude motion.
30 This induces a splitting of the energy levels which increases with increasing
31 excitation of the ν_9 vibrational mode [7]. The splitting of the energy levels is indeed
32 about 0.002 cm^{-1} for the 9^2 levels and about 0.06 cm^{-1} for the 9^3 energy levels. For
33 several other vibrational states of nitric acid involving the ν_9 mode, large amplitude
34 splittings were also evidenced by millimeter or submillimeter wave measurements
35 (see [8] and references herein). Therefore, the occurrence of large amplitude torsional
36 splittings observed in the analysis of the $2\nu_9$ band of BF_2OH was not completely a
37 surprise.
38
39
40
41
42
43
44
45
46

47 On the other hand the ν_4 (OH bending) band of HNO_3 does not reveal large
48 amplitude splittings [9] contrary to what is observed for BF_2OH . It is interesting to
49 investigate in detail this large amplitude splitting in the ν_4 band of BF_2OH , since
50 evidence for an interconversion pathway from the (lower energy, linear) HBO to the
51 (higher energy, bend) BOH radicals was predicted by recent *ab initio* calculations [10,
52 11]. This may suggest that the HBO bending mode may also be a large amplitude
53 motion for BF_2OH .
54
55
56
57
58
59
60

16/04/2007

5

2. Experimental details

2-A: Wuppertal (Germany)

Details of the synthesis of 10B (92.4 %) and 11B (99 %) and the recording of the high resolution FTIR spectra performed in Wuppertal were already given in Table 2 of Ref. [6]. Only the spectra denoted 1044 (10B) and 1043c (11B) were employed. In brief, BF_2OH was synthesized free of contaminating SiF_4 from BF_3 and H_2O in a glass-free reactor and the IR spectrum investigated in a stainless steel absorption tube measuring 1.5 m in length and outfitted with NaCl windows. The chosen total pressure was 250 Pa for 10B and 11B. A Bruker IFS 120HR interferometer was used, The resolution (1/maximum optical path difference) was adjusted to $2.4 \times 10^{-3} \text{ cm}^{-1}$.

2-B PNNL (Richland, USA)

At the Pacific Northwest National Laboratory (PNNL), the 10B and 11B spectra were recorded using a Bruker IFS 120 HR Fourier transform spectrometer. While recording rotationally-resolved combination, overtone and hot band spectra of isotopically enriched $^{10}\text{BF}_3$ and $^{11}\text{BF}_3$ samples (separately) in an adjustable pathlength White cell (Bruker A134), bands of 10B and 11B were observed. It was assumed that the 10B and 11B were produced by the reaction of $^{10}\text{BF}_3$ and $^{11}\text{BF}_3$ with residual water on the surface of the White cell.

Optical, electronic and digital filters were used to limit the spectral window. A KBr beamsplitter, Globar source, optical filter with 900 to 1300 cm^{-1} bandpass, and MCT detector were employed for these experiments. Spectra were recorded with an aperture diameter of 1.5 mm, 40 kHz scanner velocity and resolution of 0.0018 cm^{-1} . Bruker defines the maximum optical path difference (MOPD) as $0.9/\text{resolution}$, so in this case $\text{MOPD} = 0.9/0.0018 \text{ cm}^{-1} = 500 \text{ cm}$. For each isotopologue sample, 384 single-sided interferograms were coadded. For a background, a lower resolution (0.0288 cm^{-1}) spectrum was recorded of the evacuated White cell; here 512 single-sided interferograms were coadded.

For the FT conversion, a Mertz phase correction of 1 cm^{-1} and boxcar apodization were applied to the averaged interferograms. For boxcar apodization, Bruker gives the instrument linewidth as $0.61/\text{OPD} = 0.0012 \text{ cm}^{-1}$ FWHM. The

16/04/2007

6

1
2
3 averaged interferograms were post zero-filled to a factor of eight before calculating
4 the absorbance spectra.
5

6
7 The enriched $^{10}\text{BF}_3$ and $^{11}\text{BF}_3$ samples were purchased from Voltaix, Inc.,
8 each with a 99.5 atom % purity and a 99.9% chemical purity. The White cell
9 pathlength for both isotopic samples was 6.4 meters. The cell windows were CsI. The
10 pressure for the $^{10}\text{BF}_3$ sample was 261 Pa and 235 Pa for the $^{11}\text{BF}_3$ sample. Spectra
11 were recorded at room temperature, 22.5 °C. The spectrometer was evacuated to a
12 background pressure of less than 4 Pa. The spectra were wavenumber calibrated by
13 first recording a spectrum of OCS using the same instrument settings as described
14 above and then using the designated OCS calibration lines in the NIST wavenumber
15 calibration tables [12] as a reference. The average uncertainty of the OCS lines used
16 for calibration was about 0.000013 cm^{-1} , and the estimated accuracy of the calibrated
17 wavenumber is of $\sim 0.00015\text{ cm}^{-1}$.
18
19
20
21
22
23
24
25
26
27

28 3. Analyses of the $2\nu_9$ and ν_4 bands

29
30 The $2\nu_9$ and ν_4 bands of the 10B and 11B isotopic species of BF_2OH are in
31 principle hybrid bands with both A- and B-type transitions. For the $2\nu_9$ band only A-
32 type transitions were observed. On the other hand, for the ν_4 band the A-type
33 character is more pronounced than the B- type one. For A- type bands, the P and R
34 branches are structured in stacks of lines separated by $(B_z+B_x)/2$. These stacks
35 consist of $[J',d',K'_c] \leftarrow [J'',d'',K''_c]$ transitions (d denotes the degenerate K_a values with
36 $K_a=J-K_c$ or $J-K_c+1$), for given values of $(2J-K_c)$ with rather high K_c values ($K_a \ll K_c \sim J$).
37 We observed that for $2\nu_9$ and ν_4 bands each P or R transition was furthermore split
38 into two components separated by about 0.005 and 0.0035 cm^{-1} . Examples of such
39 splittings are illustrated in Figures 2 and 3 which show portions of the R branch of the
40 $2\nu_9$ band of 11B and of the P branch of the ν_4 band of 10B respectively. These
41 splittings which decrease slightly with increasing values of $(J-K_c)$ tend to vanish for
42 high values of K_a ($K_a \sim J$).
43
44
45
46
47
48
49
50
51
52
53

54 On the other hand the Q branches are congested and therefore difficult to assign
55 since they group together transitions with high K_a values ($K_c < K_a \sim J$). Figures 4 and 5
56 display various portions of the $2\nu_9$ Q branches for 10B and 11B, respectively. The
57 torsional (or bending) splittings which are almost negligible for high K_a values are
58 usually more difficult to identify in the Q branches. Nevertheless, Figures 4 and 5
59
60

16/04/2007

7

show examples of these splittings in the low frequency range of the $2\nu_9$ Q branches for ^{10}B and ^{11}B respectively. This complexity is even more dramatic for the ν_4 bands since both an A-type and a B-type component exist in the low and high frequency ranges of the Q branch, respectively (see Figure 6 for example).

Finally, it is worth noticing that the analyses were difficult since both the $2\nu_9$ and ν_4 bands are perturbed by “classical” vibration – rotation resonances.

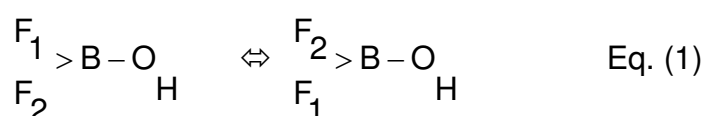
In a first step, the assignments were found by following the regular structure of doublets in the P and R branches and by checking the assignments using combination differences calculated employing the ground state parameters of Ref. [3] for both ^{10}B and ^{11}B . In order to establish the assignments, it was necessary to use the predictions of a theoretical model (see next section) which accounts for the observed “classical” vibration rotation resonances together with the perturbations linked to the large amplitude motions. In this way rather complete assignments could be performed for the $2\nu_9$ and ν_4 bands for both the ^{10}B and ^{11}B isotopic species of BF_2OH . Tables 2 and 3 report on the statistics of the assignments.

4. Hamiltonian model

4-A Symmetry properties and large amplitude motions

Before describing the Hamiltonian model which is used to calculate the energy levels of BF_2OH it is necessary to go into some details about the symmetry properties of this molecule. In its equilibrium configuration BF_2OH is a planar molecule. The corresponding point group $C_s = \{E, \sigma_{xz}\}$ (where xz is the plane of the molecule) is isomorphic to the inversion group $G^* = \{E, E^*\}$, where E^* is the laboratory-fixed inversion.

For BF_2OH , both ν_9 (torsion of the OH bond relative to the BF_2 moiety) and ν_4 (OH in plane bending) correspond to large amplitude motions which lead to the exchange of the fluorine nuclei:



16/04/2007

8

1
2
3 It can then be assumed that during this large amplitude OH torsion and/or OH
4 bending motion, the “average” conformation of the $F_2 > B-O$ frame is of C_{2v}
5 symmetry. This C_{2v} point group is isomorphic to the permutation-inversion group
6 $G_4 = \{E, E^*, (12), (12)^*\}$ where (12) is the permutation of the two fluorine nuclei F_1 and
7 F_2 and E^* is the inversion. Table 4 gives the character tables for C_{2v} and G_4 together
8 with the symmetry species of the components of the angular momentum operator \mathbf{J}
9 and of the electric dipole moment $\boldsymbol{\mu}$.
10
11
12
13
14
15

16 Let us now describe in detail the electronic, vibrational, OH- torsion, OH-bend,
17 rotational, and ^{19}F nuclear $-$ spin contributions to the symmetry properties of the total
18 wavefunctions. The ground electronic state is totally symmetric for BF_2OH , and we
19 are dealing in this study with vibrational states involving only vibrational excitation in
20 ν_9 and/or ν_4 . Because of the existence of large amplitude motions, each OH-
21 torsional 9^v /OH- bending 4^v vibrational state is split into two sublevels which are
22 referenced here as $^{\text{Low}}9^v$ and $^{\text{High}}9^v / ^{\text{Low}}4^v$ and $^{\text{High}}4^v$ for the higher and lower energy
23 subcomponent, respectively. Table 4 also gives the symmetry properties for the
24 “High” and “Low” subcomponents of each torsional 9^v or bending 4^v vibrational state:
25 these results are deduced from those described in Ref. [7]. The parity for the v
26 vibrational quantum number is relevant only for the symmetry properties of 9^v and
27 not for 4^v because ν_9 is of A'' symmetry while ν_4 is of A' symmetry. This is because ν_9
28 corresponds to the “out -of -plane” OH torsion while ν_4 (OH bending) is an “in -plane”
29 mode. In Table 4 the symmetry properties of the rotational wavefunctions $[J, K_a, K_c]$
30 which depend on the K_a and K_c parity are quoted. Finally, the permutation (12) of the
31 F_1 and F_2 fluorine nuclei leads to the permutation of the fluorine nuclear spins. For
32 ^{19}F the nuclear spin is $I=1/2$ and Table 4 gives the symmetry properties of the ^{19}F
33 fluorine nuclear spin symmetrical (resp. antisymmetrical) wavefunctions for which the
34 nuclear spin statistics give a weight of $g_n=3$ (resp. $g_n=1$).
35
36
37
38
39
40
41
42
43
44
45
46
47
48
49
50

51 Since we are dealing with $B^{19}\text{F}_2\text{OH}$ isotopic species involving the ^{19}F Fermion
52 nuclei (with a $1/2$ nuclear spin) the total wavefunctions (i.e. including the electronic,
53 vibrational, OH- torsion, OH-bend, rotational, and ^{19}F nuclear $-$ spin contributions)
54 must change sign under the permutation (12) of the two fluorine nuclei F_1 and F_2 .
55 Therefore, only the energy levels corresponding to an antisymmetrical (B_1 or B_2) total
56 wavefunction exist. As a consequence, the vibrational, OH-torsion, OH-bending,
57 rotation (vib-tors-bend-rot) energy levels with $\Gamma(\varphi_{\text{vib-tors-bend-rot}}) = A_1$ or A_2 (resp. $\Gamma(\varphi_{\text{vib-}}$
58
59
60

16/04/2007

9

1
2
3 tors-bend-rot)=B₁ or B₂) exist only when associated with the antisymmetric (resp.
4 symmetric) nuclear –spin wavefunctions with a g_n=1 (resp. g_n=3) nuclear spin
5 statistical weight.
6
7

8 The Hamiltonian matrices used for the calculation of the {9²,6¹9¹} and
9 {4¹,7¹9¹,6¹7¹} interacting energy levels split into four sub-matrices. Table 5 gives the
10 classification in four symmetry types (A₁ to B₂) of the 9^v torsion- rotation and of the 4^v
11 bending-rotation wavefunctions, according to the parity of K_c and to the nuclear spin
12 statistical weights (g_n=1 or g_n=3).
13
14

15 As far as the analyses of the spectra are concerned, only very little information
16 can be obtained concerning the energy levels with g_n=1. For example, in the P and R
17 -branches of the 2ν₉ band the assigned transitions involve 9² energy levels with high
18 K_c values (K_c ~J) for which the K_a degeneracy (K_a=d for K_a=J-K_c ⇔ K_a=J+1-K_c)
19 occurs. In this case the energy levels {(^{High}9² [J,K_a=even,K_c],g_n=3) and
20 ^{High}9²[J,K_a=odd,K_c],g_n=1)} (resp. {(^{Low}9² [J,K_a=even,K_c],g_n=3) and
21 ^{Low}9²[J,K_a=odd,K_c],g_n=1)}) coincide in energy. It is therefore not possible to observe
22 separately the transitions with g_n=1 and 3. In fact, the observed doublets (see Figure
23 2) concern the {^{High}9² [J,K_a=d,K_c]} and {^{Low}9²[J,K_a=d,K_c]} levels each of them having a
24 total statistic weight of 4 (corresponding to g_n=3 + g_n=1). The same situation occurs
25 for the P and R -branches of the ν₄ band as can be seen in Figure 3.
26
27
28
29
30
31
32
33
34
35
36

37 This K_a degeneracy does not occur for the transitions involved in the Q
38 branches. One could therefore expect to distinguish between strong (g_n=3) and weak
39 (g_n=1) transitions. Unfortunately, the torsional splittings are significantly weaker (less
40 than 0.001cm⁻¹ for K_a~J and J>18) and the identification of the weaker “g_n=1”
41 transitions is difficult since the Q branches are congested. However, the (g_n=3/g_n=1)
42 staggering effect could be observed in portions of the low frequency range of the 2ν₉
43 Q branches, as shown in Figures 4 and 5 for the 10B and 11B isotopic species
44 respectively. In this case the (g_n=3/g_n=1) staggering of the lines is obvious.
45
46
47
48
49
50

51 Of course the same situation occurs for ν₄ except that the bending splittings
52 are smaller (only ~0.0035 cm⁻¹ for the P and R branches of ν₄ instead of ~0.005 cm⁻¹
53 for 2ν₉) and the (g_n=3/g_n=1) staggering effect could be only occasionally observed in
54 the Q branches.
55
56
57
58
59
60

16/04/2007

10

4-B Classical vibration – rotation interactions

The 9² energy levels:

The 9² energy levels are perturbed through B- type and A- type Coriolis resonances with the levels of the 6¹9¹ dark state. More precisely, for 10B (11B) these rather weak resonances reach their maximum at J~62 (58) for the 9² levels with K_c=44 (43) for the 9² levels and K_c=41 (40) for 6¹9¹.

The 4¹ energy levels:

In the course of the analysis of the ν_4 band for the 10B (11B) isotopic species, we noticed that the 4¹ levels involving K_c values close to K_c=28 (25) were perturbed. Using the spectroscopic parameters determined from the analyses of the ν_7 and ν_9 bands [6] and using symmetry considerations, we identified the perturbing dark state as 7¹9¹ (A" symmetry) located around 973 cm⁻¹ (971 cm⁻¹) for 10B (11B). More explicitly, due to this B-type Coriolis resonance, levels of the 4¹ state of 10B (11B) with K_c=28 (25) are resonating with the levels of the 7¹9¹ dark state with K'_c=27 (24); the crossing of the two series occurring around J=30 (32). Since this resonance is strong and involves rather low rotational quantum numbers, some transitions for the $\nu_7+\nu_9$ dark band could be clearly identified in the spectrum near the crossing of the 4¹ and 7¹9¹ resonating series. An example illustrating these perturbations is given in Figure 3, which shows a portion of the P branch of the ν_4 band. As was mentioned previously, this ν_4 band exhibits a doublet structure which does not appear for the transitions of the resonating dark $\nu_7+\nu_9$ band. This shows that the 7¹9¹ dark state is not responsible for the large amplitude effects that affect the 4¹ energy levels.

Furthermore, an additional resonance was observed at higher energies for the ν_4 transitions involving K'_c values close to K'_c=44 (48) for 10B (11B). We identified this resonance as an anharmonic perturbation by the 6¹7¹ dark state. This perturbation involves mainly the K'_c=42 (46) levels of the 6¹7¹ state. As this rather weak resonance affects only weak ν_4 transitions, no lines belonging to the $\nu_6+\nu_7$ dark bands of both isotopes could be identified in the spectra of any of the two isotopes.

4-C Preliminary calculations

The BF₂OH spectrum exhibits some analogies to the HNO₃ spectrum:

- the 2 ν_9 bands for both species are strong

16/04/2007

11

1
2
3 - the $2\nu_9$ lines of both species are split.
4

5 On the other hand, the observation of large amplitude splittings in the analysis of the
6 ν_4 band of BF_2OH (associated to the OH bending motion) was rather unexpected as
7 compared to HNO_3 .
8

9 For nitric acid, the $2\nu_9$ overtone band (near 896 cm^{-1}) is almost as strong as the ν_5
10 band (near 879 cm^{-1}). In addition, although ν_5 (NO_2 in-plane bend) is a low amplitude
11 mode, torsional splittings were easily observed in the millimeter wave region for
12 rotational transitions of both the 9^2 the 5^1 excited states of HNO_3 [13-16]. In fact both
13 the high intensity for the $2\nu_9$ band and the existence of splittings for rotational
14 transitions in the 5^1 state could be explained satisfactorily through the existence of an
15 overall mixing of the 9^2 and 5^1 wavefunctions due to a very strong Fermi resonance
16 coupling the 9^2 and 5^1 energy levels [16].
17

18 At the start of the present study, it seemed reasonable to make the assumption that
19 strong Fermi resonances couple the 9^2 and 4^1 states of BF_2OH . Such resonances
20 might explain the strength of the $2\nu_9$ overtone band and the existence of large
21 amplitude splittings in ν_4 . Therefore, a preliminary calculation of the 9^2 and 4^1 energy
22 levels was performed assuming such resonances and using a Hamiltonian matrix
23 analogous to the one used for HNO_3 [16].
24

25 Assuming that the 9^2 and 4^1 splittings have their common physical origin in the OH
26 torsional mode (ν_9 vibrational mode), it was necessary to fix the Fermi constant term
27 to a value of about 40.3 cm^{-1} in order to reproduce the ν_4 line splittings. This proved
28 to be unrealistic since it would lead for 11B to a value of $\sim 1008.4\text{ cm}^{-1}$ for the
29 vibrational energy of the 9^2 state, which differs from the value of 1045.7 cm^{-1}
30 obtained assuming that $E_{9^2}=2E_{\nu_9}$. As a consequence, the vibrational energy of the 9^2
31 state should indeed be larger than 1045.7 cm^{-1} because ν_4 is located below $2\nu_9$. Also
32 the values obtained for the rotational constants of the 9^2 and 4^1 states were
33 unrealistic. In particular, contrary to 9^2 , for 4^1 the value of B_z was found to be smaller
34 than that of B_x . Finally, the fit was not satisfactory since, for levels with $J\leq 30$, the
35 standard deviation of the fit was already $\sim 0.007\text{ cm}^{-1}$. Clearly the assumption that the
36 ν_4 splittings originated from those of $2\nu_9$ was physically unacceptable. Therefore,
37 separate calculations had to be made for the 9^2 and 4^1 energy levels.
38
39
40
41
42
43
44
45
46
47
48
49
50
51
52
53
54
55
56
57
58
59
60

16/04/2007

12

4-D Hamiltonian matrix

The form of the Hamiltonian matrices used to calculate the energy levels are given in Tables 6-A and 6-B for the $\{9^2, 6^1 9^1\}$ and $\{4^1, 7^1 9^1, 6^1 7^1\}$ polyads of interacting states, respectively.

As was pointed out previously, various “classical” vibration – rotation resonances had to be accounted for:

- A B-type Coriolis resonance between the 9^2 and $6^1 9^1$ vibrational states.
- For the 4^1 energy levels, a B-type Coriolis resonance with the $7^1 9^1$ levels together with an additional anharmonic interaction and a C-type Coriolis resonance with $6^1 7^1$ state.

In the v- diagonal blocks, the rotational operators for each of the 9^2 , $6^1 9^1$, 4^1 , $7^1 9^1$, and $6^1 7^1$ vibrational states include XZ_v non-orthorhombic operators:

$$XZ_v = h_{xz}^v \{ J_x, J_z \} \quad \text{Eq.(2)}$$

in addition to Watson’s operators written in an I' representation with an A-type reduction [17]. These XZ_v operators account for the rather strong Coriolis interactions linking the two 9^2 torsional (or 4^1 bending) sub-states that are due to the large amplitude tunneling effects. In order to have a common reference system of axes ($X_{99}, Y_{99}, Z_{99}/X_4, Y_4, Z_4$) for the $\{9^2, 6^1 9^1/4^1, 7^1 9^1, 6^1 7^1\}$ resonating upper states, the XZ_v non-orthorhombic operators also had to be included in the rotational operators of the $6^1 9^1/7^1 9^1, 6^1 7^1$ resonating dark states. The h_{xz}^v non-orthorhombic parameters for the $6^1 9^1/7^1 9^1, 6^1 7^1$ dark states were fixed at the value derived for the interacting $9^2/4^1$ bright states.

Additionally, the tunneling splittings due to the large amplitude OH torsion (for the $2\nu_9$ band) or OH bending (for the ν_4 band) had to be accounted for by specific operators in the 9^2 and 4^1 vibrational blocks, respectively. For nitric acid, the observed torsional splittings could be successfully modeled using the Internal Axis Method (IAM) –like approach [16, 18-21]. In that approach, the general form of the IAM operator ^{IAM}H involves matrix elements of the $D(\chi, \theta, \varphi)$ Wigner's operators [22], where χ, θ , and φ are the Euler angles. Because of symmetry $\chi = \varphi + \pi$ for C_s -

16/04/2007

13

1
2
3 type planar molecules like HNO₃ or BF₂OH. Therefore only two independent angles²
4 θ and φ are actually to be considered. In the analysis of the {5¹,9²} interacting states
5 of HNO₃ [16] both the θ and φ angles could be determined together with the torsional
6 splitting parameters since a large set of rotational transitions in the 5¹ and 9² excited
7 states measured by millimeter wave techniques were included in the least squares fit
8 together with 5¹ and 9² infrared energy levels.

9
10 On the contrary, only infrared data are presently available for the 9² and 4¹ excited
11 states of BF₂OH. Therefore, it turned out that only the φ angle could be determined
12 from the least squares fits, and consequently θ was set fixed to zero during the
13 calculations.

14 The exact form of the rotational, vibration- rotational, torsional or bending operators is
15 given in Table 6.

26 5. Results

27
28 The calculations of the {9²,6¹9¹} and {4¹,7¹9¹,6¹7¹} resonating energy levels of
29 10B and 11B were performed using the Hamiltonian models given in Table 6,
30 sections A and B respectively. For 10B (11B) the Hamiltonian constants resulting
31 from the least squares fits of the experimental data are given together with their
32 estimated uncertainties in Table 7 (8) and Table 9 (10) for the {9²,6¹9¹} and
33 {4¹,7¹9¹,6¹7¹} resonating levels respectively.

34 For 10B (11B) Table 2 (3) gathers details of the energy level calculations in terms of
35 standard deviations and statistical analyses. It is clear that the results are excellent
36 for both the {9²,6¹9¹/4¹,7¹9¹,6¹7¹} resonating states. The quality of the calculations is
37 furthermore proved by the consistency of the parameters derived for the 10B and
38 11B isotopic species.

39
40
41
42
43
44
45
46
47
48
49
50
51
52
53
54
55
56
57 ² By convention, the BF₂ moiety is defined as the rotor and the OH bond as the frame
58 and the φ angles are related to the rotor and frame moments of inertia by
59

$$60 \quad 2\varphi = 180^\circ \frac{I_{\text{Rotor}}}{I_{\text{Rotor}} + I_{\text{Frame}}}.$$

16/04/2007

14

6. Discussion

In this section we discuss problems concerning the values of the centrifugal distortion constants, the signs of some Hamiltonian constants and the definition of the angles involved in the torsional or bending operators.

6-A Values of the centrifugal distortion constants for the bright states

In Tables 7-10, some of the centrifugal distortion constants for the 9^2 and 4^1 bright states differ significantly from the ground state values: this is because insufficient information is available for the 6^19^1 and 6^17^1 dark states.

6-B Signs of the parameters

As it was discussed in detail by Perrin et al. [16], absolute signs can be determined from the least squares fit only for some of the parameters quoted in Tables 7-10. For example, the signs of the torsional h^{TORS} or bending h^{BEND} constants together with all the parameters appearing in the orthorhombic part of the rotational Hamiltonians (i.e. the Watson's A-type expansion) are obtained from the fit. On the other hand, as usual, the signs of the higher order constants occurring in the $6^19^1 \leftrightarrow 9^2$ B-type, $7^19^1 \leftrightarrow 4^1$ B-type, $6^17^1 \leftrightarrow 4^1$ C-type Coriolis or $6^17^1 \leftrightarrow 4^1$ anharmonic operators are obtained only relative to the lower order constants (${}^{69,99}B_x$, ${}^{79,4}B_x$, ${}^{67,4}C_{xz}$ and ${}^{67,4}Anh_{xy}$ in the present case (see Table 6)). As a consequence, any of the following changes of sign leave the energy of the levels unchanged:

- For the $\{9^2, 6^19^1\}$ interacting states:

$$\begin{aligned} & \text{TORS}_\varphi \rightarrow -\text{TORS}_\varphi \\ & \text{or } {}^{69,99}B_x \rightarrow -{}^{69,99}B_x \\ & \text{or } h_{xz}^{99} \rightarrow -h_{xz}^{99} \quad (h_{xz}^{69} = h_{xz}^{99}) \end{aligned} \quad \text{Eqs. (3)}$$

- For the $\{4^1, 7^19^1, 6^17^1\}$ interacting states:

$$\begin{aligned} & \text{BEND}_\varphi \rightarrow -\text{BEND}_\varphi \\ & \text{or } {}^{79,4}B_x \rightarrow -{}^{79,4}B_x \\ & \text{or } ({}^{67,4}C_{xz} \rightarrow -{}^{67,4}C_{xz} \quad \underline{\text{and}} \quad {}^{67,4}Anh_{xy} \rightarrow -{}^{67,4}Anh_{xy}) \\ & \text{or } h_{xz}^4 \rightarrow -h_{xz}^4 \quad (h_{xz}^{67} = h_{xz}^{79} = h_{xz}^4) \end{aligned} \quad \text{Eqs. (4)}$$

16/04/2007

15

6-C Axis switching effects

The signs chosen for the h_{xz}^{99} and h_{xz}^4 parameters that appear in the XZ_v non-orthorhombic terms (see Eq. 2 and Table 6) lead to an anti-clockwise rotation of the (a,b,c) initial system around the c-axis which results in the non-orthorhombic ($X_{99}, Y_{99}, Z_{99}/X_4, Y_4, Z_4$) reference system of axes for the $\{6^1 9^1, 9^2/4^1, 7^1 9^1, 6^1 7^1\}$ resonating states respectively. The rotation angle α_v (see Figure 1) is given by [16]:

$$\alpha_v \approx 1/2 \operatorname{atan} \left(\frac{-2h_{xz}^v}{(B_z^v - B_x^v)} \right) \quad \text{Eq. (5)}$$

with $v=99/4$ for $\{9^2, 6^1 9^1/4^1, 7^1 9^1, 6^1 7^1\}$.

According to the values of the h_{xz}^v , B_z^v and B_x^v constants (Tables 7-10), these angles are:

$$\alpha_{99} \approx 35.5(10)^\circ \quad (\alpha_{99} \approx 35.4(10)^\circ) \quad \text{Eqs. (6)}$$

for the $\{9^2, 6^1 9^1\}$ states of 10B(11B), and:

$$\alpha_4 \approx 17.91(3)^\circ \quad (\alpha_4 \approx 15.37(6)^\circ) \quad \text{Eqs. (7)}$$

for the $\{4^1, 7^1 9^1, 6^1 7^1\}$ states of 10B(11B).

The large differences between the α_v values for the two polyads show that the large amplitude OH- torsion and the large amplitude OH-bending motion cannot be accounted for simultaneously. This is confirmed by the fact that the splittings for the $J=0$ levels are very different for the torsion ($^{99}\text{Split}^{\text{TORSE}} \cong 5.1 \times 10^{-3} \text{ cm}^{-1}$) and for the bending ($^4\text{Split}^{\text{BEND}} \cong 3.7 \times 10^{-3} \text{ cm}^{-1}$).

Finally, as we will see in the next Section, this rather strong axis switching effect has to be considered properly if reliable line intensities are to be calculated.

16/04/2007

16

7. Simulation of the experimental spectra

To emphasize the quality of the calculations we have compared the observed and calculated spectra in various spectral regions. The line positions were generated using the ground state constants from [3] and the upper state constants given in Tables 7-10 of this paper.

7-A Line intensity calculations

It should be stressed that only relative intensities were computed since no attempt was made to derive absolute experimental intensities.

The intensity of a line [23, 24] is proportional to R_A^B which is the square of the matrix element of the transformed transition moment operator μ_Z' :

$$R_A^B = \left| \left\langle v', J' K'_a K'_c \left| \mu_Z' \right| 0, J'' K''_a K''_c \right\rangle \right|^2 \quad \text{Eq.(8)}$$

where μ_Z' is the transformed dipole moment operator [23, 24], which can be expanded as

$$\mu_Z' = \sum_{v' \in B'} |0\rangle \nu \mu_Z' \langle v'| \quad \text{Eq.(9)}$$

where v' belongs to the upper $B' = \{9^2, 6^1 9^1\}$ or $\{4^1, 7^1 9^1, 6^1 7^1\}$ polyad of interacting states. For the $2\nu_9$ and ν_4 bright bands, both A-type and B-type transitions are allowed for symmetry reasons. Therefore, up to first order, the expansion of the $2\nu_9$ and ν_4 transition moment operators can be written as [23, 24]:

$$\nu \mu_Z = \varphi_Z \nu \mu_Z^1 + \varphi_X \nu \mu_X^1 + \dots \quad \text{Eq.(10)}$$

where φ_Z and φ_X stand for the direction cosines ϕ_{ZZ} and ϕ_{ZX} respectively.

In the usual calculations the upper and ground state rovibrational wavefunctions are expanded as on the Wang's type sub-bases (see Table 6):

16/04/2007

17

$$|v', J' K'_a K'_c\rangle = \sum_{v' \in B'} \sum_{K', \gamma'} C_{v'}^{\gamma' K'} |v'\rangle |J' K' \gamma'\rangle \quad \text{Eq.(11)}$$

$$|v=0, J K_a K_c\rangle = \sum_{K''} C_0^{\gamma'' K''} |J K'' \gamma''\rangle \quad \text{Eq.(12)}$$

In Eqs.(11) and (12), the $C_{v'}^{\gamma' K'}$ and $C_0^{\gamma'' K''}$ coefficients are obtained from the diagonalization of the Hamiltonian matrices.

However, as for HNO_3 [16], it is necessary to account properly for the axis switching effects. Indeed, for both 10B and 11B isotopologues of BF_2OH , the $(X_{99}, Y_{99}, Z_{99}/X_4, Y_4, Z_4)$ reference axes for the upper $\{9^2, 6^1 9^1/4^1, 7^1 9^1, 6^1 7^1\}$ vibrational excited states are tilted anticlockwise around the c axis by about $\alpha_{99} \sim 35.4^\circ / \alpha_4 \sim 16.6^\circ$ from the (a,b,c) inertial axes (see Fig.(1)). To the contrary, the ground vibrational state wave functions are calculated using a standard I' Watson A-type Hamiltonian and the reference axes are the (a,b,c) inertial axes of the molecule [17]. To solve this problem it is necessary to re-write the ground state wavefunctions so that they are consistent with the upper state wavefunctions.

$$|v=0, J K_a K_c\rangle = \sum_{\substack{K'' \gamma'' \in \{E^+, O^-\} \\ \text{or } K'' \gamma'' \in \{E^-, O^+\}}} \alpha_v C_0^{\gamma'' K''} |^{\alpha_v} J'' K'' \gamma''\rangle. \quad \text{Eq.(13)}$$

This new expansion is performed simultaneously on both the E^+ and O^- (resp. on both the E^- and O^+) sub-blocks of the Wang bases (see Table 6) whereas in Eq.(12) the summation on K'' is performed on only one of the four sub-blocks of the Wang bases $\{|J, K, \gamma\rangle = E^+ \text{ or } E^- \text{ or } O^+ \text{ or } O^-, \text{ with } E^\pm \text{ for } K=\text{even} \text{ and } O^\pm \text{ for } K=\text{odd} \text{ and } \gamma = \pm 1\}$.

The relationship between the two expansions of the ground state wavefunctions is obtained using the Wigner tensorial approach [22] and the $d_{K', K''}^{(J)}(\alpha_0)$, matrix elements (see details in Ref. [16]):

16/04/2007

18

$$\alpha_v C_0^{\gamma'K'} = \sum_{K''} C_0^{\gamma''K''} \left(d_{K',K''}^{(J)}(\alpha_v) + \gamma' (-1)^{K'-K''} d_{K',-K''}^{(J)}(\alpha_v) \right) \quad \text{Eq. (14)}$$

(with $\alpha_v = \alpha_{99} / \alpha_v = \alpha_4$ for the $\{9^2, 6^1 9^1 / 4^1, 7^1 9^1, 6^1 7^1\}$ polyad).

We have used this formalism to calculate the line intensities for the two studied polyads of interacting bands. As $2\nu_9$ and ν_4 are in principle A and B hybrid – type bands, the transition moments operators involve both the ${}^v\mu_z^1$ and ${}^v\mu_x^1$ parameters defined in the switched axis system (x,y,z) (Eq. (10)). These parameters are related to the transition moment operator parameters in the principal axis system (a,b,c) through:

$$\begin{aligned} {}^v\mu_a^1 &= \cos \alpha_v {}^v\mu_z^1 - \sin \alpha_v {}^v\mu_x^1 \\ {}^v\mu_b^1 &= \sin \alpha_v {}^v\mu_z^1 + \cos \alpha_v {}^v\mu_x^1 \end{aligned} \quad \text{Eq. (15)}$$

with $v=99$ or 4 .

For the dark bands $\nu_6+\nu_9$, $\nu_7+\nu_9$ and $\nu_6+\nu_7$ the transition moments were set to zero.

For the bright $2\nu_9$ band, only A-type transitions were observed. Therefore, for $2\nu_9$ the transition moment operator is parallel to the a- inertial axis (see Figure 1), and the $2\nu_9$ line intensities could be satisfactorily reproduced using the following ratio for the z- and x- component of the $2\nu_9$ transition moment operator (using $\alpha_{99} \approx 35.4^\circ$ for 10B and 11B):

$${}^{99}\mu_x^1 / {}^{99}\mu_z^1 = -\tan(\alpha_{99}) \approx -0.711 \quad \text{Eq. (16)}$$

For the bright ν_4 band, the problem is more difficult since both A- and B- type transitions were observed. In this case, from examination of the spectra and fitting a few relative line intensities, we estimate the ratio of the z- to x- components of the ν_4 transition moment operator to be:

$${}^4\mu_x^1 / {}^4\mu_z^1 \approx +0.71 \pm 20\% \quad \text{Eq. (17)}$$

16/04/2007

19

When using $\alpha_4 \approx 16.6^\circ$ for 10B and 11B, this leads to the ratio for the b- to a-components of the ν_4 transition moment operator:

$${}^4\mu_b^1 / {}^4\mu_a^1 \approx +1.28 \pm 20\% \quad \text{Eq. (18),}$$

which is in good agreement with the *ab initio* prediction [3,25]:

$$\left({}^4\mu_b^1 / {}^4\mu_a^1 \right)^{Ab\ initio} \approx 1.05 \quad \text{Eq.(19).}$$

7-B Comparison between the experimental and calculated spectra

In Figures 2-7 we compare the observed and calculated spectra in various spectral regions, where different type of resonances were observed.

Figures 2 and 3 show a portion of the R branch of the $2\nu_9$ band of 11B and of the P branch of the ν_4 band of 10B illustrating examples of torsional and bending splittings. In Figure 3, the resonance involving the 4^1 and $7^1 9^1$ energy levels for $K'_c \sim 28$ is clearly seen, and lines from the dark $\nu_7 + \nu_9$ resonating band appear in spite of the corresponding transition moment fixed to zero.

Figures 4 and 5 show portions of the Q branch of the $2\nu_9$ band for 10B and 11B respectively. In Figure 5, the “staggering” effect, which is due to the ($g_n=3/g_n=1$) nuclear spin statistical weights, is clearly observable. Figures 6 and 7 give portions of the Q branch for the ν_4 band of 10B and 11B respectively: the A- and B- type character of the ν_4 band is obvious.

In all cases, the agreement between the observed and calculated s is very satisfactory proving the quality of the model both in terms of line positions and of line intensities.

8. Conclusion:

From high resolution Fourier transform spectra of ^{10}B - and ^{11}B enriched as well as of natural samples of BF_2OH the first rovibrational analysis of the $2\nu_9$ and ν_4 bands for $^{10}\text{BF}_2\text{OH}$ and $^{11}\text{BF}_2\text{OH}$ has been performed up to very high quantum

16/04/2007

20

1
2
3 numbers. Numerous perturbations were observed in the analysis and were
4 accounted for in the Hamiltonian model. First, the $2\nu_9$ bands and ν_4 bands are
5 perturbed by classical vibration – rotation resonances. More explicitly B- type Coriolis
6 interactions couple the 9^2 and 4^1 energy levels with those of the 6^19^1 and 7^19^1 dark
7 states, respectively. Also, anharmonic and C-type Coriolis interactions link the 4^1
8 energy levels with those of the dark 6^17^1 state. Most prominently, large amplitude
9 effects were observed for the $2\nu_9$ and ν_4 bands, leading to splittings of the energy
10 levels of about 0.005 and 0.0035 cm^{-1} for the 9^2 and 4^1 states respectively. These
11 splittings are easily observable in the P and R branches for both bands. The
12 theoretical model used to reproduce the experimental energies accounts for the
13 “classical” vibration –rotation resonances as well as for the large amplitude torsional
14 (or bending) effects. The latter were interpreted using an IAM (Internal Axis Method) -
15 like approach. In this approach the Coriolis resonances between the two torsional (or
16 bending) substates were taken into account by means of $\{J_x, J_z\}$ non-orthorhombic
17 terms in the Hamiltonian v-diagonal blocks. As a consequence, the z-quantification
18 axis deviates from the a inertial axis with an axis switching effect of $\sim 35^\circ / \sim 16.6^\circ$ for
19 the $\{9^2, 6^19^1/4^1, 7^19^1, 6^17^1\}$ polyad of interacting vibrational states.
20

21 From the observation of different splittings and axis switching effects one can then
22 conclude that both the OH- torsion and the OH-bending modes have to be
23 considered as large amplitude motions. Finally, the experimental spectra were
24 simulated very satisfactorily by considering both the above mentioned effects and
25 the intensity alternation due to the large amplitude motions which cause an
26 exchange of the two fluorine nuclei. .
27
28
29
30
31
32
33
34
35
36
37
38
39
40
41
42
43
44
45
46
47
48
49

Acknowledgments

50 We thank the Deutsche Forschungsgemeinschaft and the French C.N.R.S. (Centre
51 National de la Recherche Scientifique) for financial support via the project CERC3.
52 Furthermore, the initial work was supported by the European Community within the
53 SPHERS network (contract HPRN-CT-2000-00022). Also, we are indebted to the
54 Laboratoire Associé “HIRES” for financial support. Part of the research described
55 here was performed in the Environmental Molecular Sciences Laboratory, a National
56 Scientific User Facility sponsored by the Department of Energy's Office of Biological
57
58
59
60

16/04/2007

21

1
2
3 and Environmental Research and located at the Pacific Northwest Laboratory. The
4 Pacific Northwest National Laboratory is operated for the United States Department
5 of Energy by Battelle Memorial Institute under contract number AC05-76RLO-1830.
6
7 Finally, we thank Mrs. Marion Litz for valuable help.
8
9
10
11
12
13
14
15
16
17
18
19
20
21
22
23
24
25
26
27
28
29
30
31
32
33
34
35
36
37
38
39
40
41
42
43
44
45
46
47
48
49
50
51
52
53
54
55
56
57
58
59
60

For Peer Review Only

16/04/2007

22

References

- [1] H.Takeo and R.H. Curl, *J. Chem. Phys.* **56**, 4314-4317 (1972).
- [2] K. Vormann, and H. Dreizler, *Z. Naturforsch.* **44a**, 1191-1195 (1989).
- [3] J. Breidung, J. Demaison, J.-F. D'Eu, L. Margulès, D. Collet, E.B. Mkadmi, A. Perrin and W. Thiel, *J. Mol. Spectrosc.* **228**, 7-22 (2004).
- [4] M.E. Jacox, K.K. Irikura, and W.E. Thomson, *J. Chem. Phys.* **113**, 5705-5715 (2000).
- [5] D.Collet, A.Perrin, H.Bürger and J.-M.Flaud, *J. Mol. Spectrosc.* **212**, 118-124 (2002).
- [6] A.Perrin, M.Carvajal-Zaera, Z.Dutkiewicz, J.-M.Flaud, D.Collet, H.Bürger, J.Demaison, F.Willaert, H.Mäder, and N.W.Larsen, *Mol. Phys.* **102**, 1641-1652 (2004).
- [7]: "High resolution Infrared Spectroscopy and One Dimensional Large Amplitude Motion in Asymmetric Tops: HNO₃ and H₂O₂", J.-M.Flaud and A.Perrin, Chap 7 in "Vibration-Rotational Spectroscopy & Molecular Dynamics", 396-460, in "Advanced Series in Physical Chemistry", D.Papoušek editor, World Scientific Publishing Company, Singapore (1997).
- [8] D.T.Petkie, P.Helminger, M.Behnke, I.R.Medvedev and F.C. De Lucia, *J. Mol. Spectrosc.*, **233**, 189-196 (2005).
- [9] A.Perrin, O.Lado-Bordowski, and A. Valentin, *Mol. Phys.* **67**, 249-270 (1989).
- [10] T. K. Ha, J. Makarewicz, *Chemical Physics Letters* **299** 637-42 (1999).
- [11] Qian-Peng, Yubin-Wang, Bing-Suo, Qizhen-Shi, and Zhenyi-Wen, *J. Chem. Phys.* **121**, 778-782 (2004).
- [12] A.G.Maki and J.S.Wells, (1998), *Wavenumber Calibration Tables from Heterodyne Frequency Measurements* (version 1.3). [Online] Available: <http://physics.nist.gov/wavenum> [2006, November 24]. National Institute of Standards and Technology, Gaithersburg, MD.
- [13] C.D.Paulse, L.H.Coudert, T.M.Goyette, R.L.Crownover, P.Helminger and F.C.De Lucia, *J. Mol. Spectrosc.* **177**, 9-18 (1996).
- [14] T.M.Goyette, L. C.Oesterling, D.T.Petkie, R.A.Booker, P.Helminger and F.C.De Lucia, *J. Mol. Spectrosc.* **175**, 395-410 (1996).
- [15] D.T.Petkie, T.M.Goyette, P.Helminger, H.M.Pickett and F.C.De Lucia, *J. Mol. Spectrosc.* **208**, 121-135 (2001).

16/04/2007

23

- 1
2
3 [16] A.Perrin, J.Orphal, J.-M.Flaud, S.Klee, G.Mellau, H. Mäder, D.Walbrodt and
4 M.Winnewisser, *J. Mol. Spectrosc.* **228**, 375-391 (2004).
5
6 [17] "Aspects of quartic and sextic centrifugal effects on rotational energy levels"
7 J.K.G.Watson, Chap 1, in "Vibrational spectra and structure", J.Durig editor,
8 Elsevier, (1977).
9
10 [18] J.T.Hougen, *J. Mol. Spectrosc.* **114**, 395-426 (1985).
11
12 [19] L.H.Coudert and J.T.Hougen, *J. Mol. Spectrosc.* **130**, 86-119 (1988).
13
14 [20] L.H.Coudert and J.T.Hougen, *J. Mol. Spectrosc.* **139**, 259-277 (1990).
15
16 [21] L.H.Coudert and A.Perrin, *J. Mol. Spectrosc.* **172**, 352-368 (1995).
17
18 [22] A.R.Edmonds, "Angular Momentum in Quantum Mechanics", Princeton
19 University Press, Princeton, NJ, (1960).
20
21 [23]"Water Vapour Line Parameters from Microwave to Medium Infrared",
22 J.-M.Flaud, C.Camy-Peyret, and R.A.Toth, Pergamon press, Oxford (1981).
23
24 [24]"Vibration-rotation dipole moment operator for asymmetric rotors",
25 C.Camy-Peyret, and J.-M.Flaud; in "Molecular Spectroscopy Modern Research"
26 (K.Narahari Rao Ed.), p. 69-110 Vol. 3, Academic Press, New York, (1985).
27
28 [25] J.Breidung, private communication (2006).
29
30
31
32
33
34
35
36
37
38
39
40
41
42
43
44
45
46
47
48
49
50
51
52
53
54
55
56
57
58
59
60

16/04/2007

24

Figure Captions:**Figure 1:**

Structure of the BF_2OH molecule and definition of the axes.

Note:

Because of the existence of non-orthorhombic terms in the v -diagonal blocks of the $\{9^2, 6^1 9^1 / 4^1, 7^1 9^1, 6^1 7^1\}$ Hamiltonians, the $(x_{99}, z_{99} / x_4, z_4)$ systems of axes differ significantly from the (b, a) inertial system. The out-of-plane y_4 and y_{99} reference axes coincide with the c inertia axis. Also the directions of the $2\nu_9 / \nu_4$ transition moment operators ${}^{99}\mu / {}^4\mu$ are indicated.

Figure 2:

Portion of the R branch of the $2\nu_9$ band of ${}^{11}\text{BF}_2\text{OH}$ (spectrum recorded at Wuppertal).

Note:

The triangles indicate the split lines which belong to the $(2J' - K'_c = 43)$ stack.

Figure 3:

Portion of the P branch of the ν_4 band of ${}^{10}\text{BF}_2\text{OH}$ (spectrum recorded at PNNL).

Note:

The triangles indicate the split lines which belong to the $(2J' - K'_c = 28)$ stack. The assignments indicate the K'_c values. A resonance of the 4^1 energy levels with those of $7^1 9^1$ is clearly visible for K'_c values near $K'_c = 28$. Due to this resonance, unsplit transitions belonging to the $\nu_7 + \nu_9$ (dark) resonating band are observed.

Figure 4:

Portion of the central part of the Q branch of the $2\nu_9$ band of ${}^{10}\text{BF}_2\text{OH}$ (spectrum recorded at Wuppertal).

Note:

Assignments are given for the ${}^Q Q_{K'_a''=J, K'_c''=0}$ transitions (black dots). For the

${}^Q Q_{K'_a''=J-2, K'_c''=2}$ branch, the transitions with nuclear spin statistical weights $g_n=3$ and

16/04/2007

25

1
2
3 $g_n=1$ are identified by open and black diamonds, respectively. The staggering effect
4 is visible.
5
6
7

Figure 5:

8
9
10 Portion of the Q branch of the $2\nu_9$ band of $^{11}\text{BF}_2\text{OH}$ (spectrum recorded at
11 Wuppertal).
12
13

Note:

14
15
16 Assignments are given for the ${}^{\circ}\text{Q}_{K_a''=J-1, K_c''=2}$ branch (with $\Delta K_a = -2$, $\Delta K_c = +1$). The
17
18

19 $g_n=3$ and $g_n=1$ transitions are identified by open and black diamonds, respectively.
20 The staggering effect is visible.
21
22
23

Figure 6:

24
25
26 Overview of the ν_4 Q branch for $^{10}\text{BF}_2\text{OH}$ (spectrum recorded at PNNL).
27
28
29
30
31

Figure 7:

32
33
34 Central part of the ν_4 Q branch for $^{11}\text{BF}_2\text{OH}$ (spectrum recorded at Wuppertal).
35
36
37
38
39
40
41
42
43
44
45
46
47
48
49
50
51
52
53
54
55
56
57
58
59
60

16/04/2007

26

Table Captions

Table 1:

Infrared bands of BF_2OH (cm^{-1})

Note:

^aA' and A'' are the symmetry species in the C_s point group.

^bMatrix band centers from Ref.[4].

^cGas phase band centers from Ref. [6].

^dThis work.

Table 2:

Range of quantum numbers for energy levels probed by infrared transitions and statistical analysis of the results of the energy level calculations for the 9^2 , 4^1 , and $7^1 9^1$ vibrational States of $^{10}\text{BF}_2\text{OH}$.

Table 3:

Range of quantum numbers for energy levels probed by infrared transitions and statistical analysis of the results of the energy level calculations for the 9^2 , 4^1 , and $7^1 9^1$ vibrational States of $^{11}\text{BF}_2\text{OH}$.

Table 4:

Character tables for the C_{2v} and G_4 symmetry groups.

Note:

Meaning of the different columns:

- J_x, J_y, J_z and μ_x, μ_y, μ_z : molecular fixed components of \vec{J} and $\vec{\mu}$ respectively.
- J_z and μ_z : Z-laboratory fixed components of \vec{J} and $\vec{\mu}$ respectively.
- Torsion and Bend: Symmetry properties for the $^{Low}9^v$ and $^{High}9^v$ (large amplitude torsion) and $^{Low}4^v$ and $^{High}4^v$ (large amplitude bend) vibrational substates.
- v: parity of v (e=even, o=odd).

16/04/2007

27

- [J K_a K_c]: symmetry of a rotational energy level according to the K_a and K_c parity (e=even, o=odd).
- Nuclear spin: symmetry properties of the nuclear spin wavefunctions attached to the fluorine nuclei (I=1/2). The symmetrical (resp. antisymmetrical) wavefunctions have nuclear spin degeneracy of g_n=3 (resp. g_n=1).
- The symbols ^{Low}g^v and ^{High}g^v / ^{Low}4^v and ^{High}4^v designate the higher and lower energy subcomponent, respectively, of each OH- torsional 9^v/OH- bending 4^v vibrational state

Table 5a) Symmetry properties of the 9^v OH torsion -rotation wavefunctions (Γ_{Tors-Rot})b) Symmetry properties of the 4^v OH-bending -rotation wavefunctions (Γ_{Bend-Rot})Note:

Meaning of the different columns:

- g_n : nuclear spin statistical weights
- K_a and K_c: parity of K_a and K_c (e=even, o=odd).
- ^{Low}g^v and ^{High}g^v / ^{Low}4^v and ^{High}4^v : higher and lower energy subcomponent, respectively, of each OH- torsional 9^v/OH- bending 4^v vibrational state

Table 6

Hamiltonian matrices and operators.

Table 7Hamiltonian constants (in cm⁻¹) for the {9²,6¹9¹} polyad of ¹⁰BF₂OHNote:

The quoted errors are one standard deviation.

^a From Ref. [3],^b Fixed to the ground state value.**Table 8**Hamiltonian constants (in cm⁻¹) for the {9²,6¹9¹} polyad of ¹¹BF₂OH

16/04/2007

28

Note:

The quoted errors are one standard deviation.

^a From Ref. [3],

^b Fixed to the ground state value.

Table 9

Hamiltonian constants (in cm^{-1}) for the $\{4^1, 7^1 9^1, 6^1 7^1\}$ polyad of $^{10}\text{BF}_2\text{OH}$

Note:

The quoted errors are one standard deviation.

^b Fixed to the ground state value [3].

Table 10

Hamiltonian constants (in cm^{-1}) for the $\{4^1, 7^1 9^1, 6^1 7^1\}$ polyad of $^{11}\text{BF}_2\text{OH}$

Note:

The quoted errors are one standard deviation.

^b Fixed to the ground state values [3].

16/04/2007

29

Table 1Infrared bands of BF₂OH (cm⁻¹)

Vibrational assignment ^a	Description	¹⁰ BF ₂ OH	¹¹ BF ₂ OH
ν_1, A'	ν (OH)	3712.5 ^b	3712.5 ^b
ν_2, A'	ν_{as} (BF)	1515.8 ^b	1464.3 ^b
ν_3, A'	ν_s (BF)	1456.9 ^b	1414.9 ^b
ν_4, A'	δ (BOH) i.p.	961.74 ^d	961.49 ^d
ν_5, A'	δ (BF ₂) i.p.	880.64 ^c	880.74 ^c
ν_6, A'	ν (F ₂ BO) i.p.		479.17 ^c
ν_7, A'	δ (F ₂ BO) i.p.		446.54 ^c
ν_8, A''	δ (F ₂ BO) o.p.	711.41 ^c	684.16 ^c
ν_9, A''	δ (BOH) o.p.	523.04 ^c	522.87 ^c
$2\nu_9, A'$		1043.89 ^d	1042.87 ^d

16/04/2007

30

Table 2

Range of quantum numbers for energy levels probed by infrared transitions and statistical analysis of the results of the energy level calculations for the 9^2 , 4^1 , and $7^1 9^1$ vibrational States of $^{10}\text{BF}_2\text{OH}$.

Vibrational states:	9^2	4^1	$7^1 9^1$
Number of lines	3958	4259	116
J and K_a ranges	$J \leq 64, K_a \leq 49$	$J \leq 65, K_a \leq 46$	$J \leq 54, K_a \leq 48$
Number of levels	1679	1571	55
$0.0 \times 10^{-3} \leq \delta < 0.5 \times 10^{-3} \text{ cm}^{-1}$	86.8%		71.9%
$0.5 \times 10^{-3} \leq \delta < 1.0 \times 10^{-3} \text{ cm}^{-1}$	9.8%		21.2%
$1.0 \times 10^{-3} \leq \delta < 3.0 \times 10^{-3} \text{ cm}^{-1}$	3.4%		6.9%
Standard deviation (10^{-3} cm^{-1})	0.42		0.57

$$\delta = |E_{obs} - E_{calc}|$$

16/04/2007

31

Table 3

Range of quantum numbers for energy levels probed by infrared transitions and statistical analysis of the results of the energy level calculations for the 9^2 , 4^1 , and 7^1 9^1 vibrational States of $^{11}\text{BF}_2\text{OH}$.

Vibrational states:	9^2	4^1	7^1 9^1
Number of lines	5381	4665	258
J and K_a ranges	$J \leq 64, K_a \leq 49$	$J \leq 69, K_a \leq 35$	$J \leq 38, K_a \leq 15$
Number of levels	2044	1687	111
$0.0 \times 10^{-3} \leq \delta < 0.5 \times 10^{-3} \text{ cm}^{-1}$	82.6%		60.9%
$0.5 \times 10^{-3} \leq \delta < 1.0 \times 10^{-3} \text{ cm}^{-1}$	12.5%		26.9%
$1.0 \times 10^{-3} \leq \delta < 2.0 \times 10^{-3} \text{ cm}^{-1}$	4.0%		9.1%
$2.0 \times 10^{-3} \leq \delta < 4.0 \times 10^{-3} \text{ cm}^{-1}$	0.9%		3.1%
Standard deviation (10^{-3} cm^{-1})	0.50		0.84

$$\delta = |E_{obs} - E_{calc}|$$

16/04/2007

32

Table 4

Character tables for the C_{2v} and G_4 symmetry groups.

					Torsion	Bend	[J K _a K _c]	Nuclear Spin
					Low g^v , High g^v	Low 4^v , High 4^v	K _a K _c Parities	
G_4	E	(12)	(12) [*]	E [*]				
C_{2v}	E	C_{2z}	σ_{yz}	σ_{xz}				
A_1	1	1	1	1	J_z μ_z	v=e Low	Low	e e Sym: $g_n=3$
A_2	1	1	-1	-1	μ_z J_z	v=0 High		e o
B_1	1	-1	1	-1	μ_y, J_x	v=0 Low		o o Antisym: $g_n=1$
B_2	1	-1	-1	1	μ_x, J_y	v=e High	High	o e

16/04/2007

33

Table 5

a) Symmetry properties of the 9^v OH torsion -rotation wavefunctions

$\Gamma_{\text{Tors-Rot}}$	g_n	OH -Torsion: 9^v $v=\text{even}$			OH -Torsion: 9^v $v=\text{odd}$		
		K_c	K_a		K_c	K_a	
			Low g^v	High g^v		Low g^v	High g^v
B_2	3	e	o	e	o	e	o
B_1	3	o	o	e	e	e	o
A_1	1	e	e	o	o	o	e
A_2	1	o	e	o	e	o	e

b) Symmetry properties of the 4^v OH-bending -rotation wavefunctions:

$\Gamma_{\text{Bend-Rot}}$	g_n	K_c	4^v OH-bending	
			K_a	
			Low 4^v	High 4^v
B_2	3	e	o	e
B_1	3	o	o	e
A_1	1	e	e	o
A_2	1	o	e	o

16/04/2007

34

Table 6

A: Hamiltonian matrix for the resonating $\{9^2, 6^1 9^1\}$ energy levels

	9^2	$6^1 9^1$
9^2	$E_{99} + H_{99}^{\text{ROT}} + H_{99}^{\text{TORS}}$	c.c.
$6^1 9^1$	$69,99_B$	$E_{69} + H_{69}^{\text{ROT}}$

B: Hamiltonian matrix for the resonating $\{4^1, 7^1 9^1, 6^1 7^1\}$ energy levels

	4^1	$7^1 9^1$	$6^1 7^1$
4^1	$E_4 + H_4^{\text{ROT}} + H_V^{\text{BEND}}$	c.c.	c.c.
$7^1 9^1$	$79,4_B$	$E_{79} + H_{79}^{\text{ROT}}$	
$6^1 7^1$	$67,4_{\text{Anh}+} 67,4_C$		$E_{67} + H_{67}^{\text{ROT}}$

v-diagonal operators **E_v = vibrational energy****The H_v^{ROT} rotational operator**

$$H_v^{\text{ROT}} = W_v + XZ_v$$

 W_v = Watson's A- type operators (I^r representation)

$$W_v = B_z^v J_z^2 + B_x^v J_x^2 + B_y^v C_v J_y^2 - \Delta_K^v J_z^4 - \Delta_{JK}^v J_z^2 J_x^2 - \Delta_J^v J_z^4 - 2\delta_J^v J_z^2 J_{xy}^2 - \delta_K^v \{J_z^2, J_{xy}^2\} + \dots$$

 XZ_v = non orthorhombic terms

$$XZ_v = h_{xz}^v \{J_x, J_z\} + \dots$$

16/04/2007

35

Torsion (in 6-A) or bending (in 6-B)

$$\langle JK'\gamma' | I^{AM} H | JK''\gamma'' \rangle = \varepsilon(-1)^{K'} \left(\cos((K'+K'')\varphi) d_{K',K''}^{(J)}(\theta) + \gamma'' \cos((K'-K'')\varphi) d_{K',-K''}^{(J)}(\theta) \right)$$

For $\theta=0$ (see text) this expression leads to:

$$\text{In A: } \langle JK'\gamma' | H^{\text{TORS}} | J K''=K' \gamma''=\gamma' \rangle = \varepsilon h^{\text{TORS}} (-1)^{K'} \cos(2K'\varphi^{\text{TORS}})$$

$$\text{In B: } \langle JK'\gamma' | H^{\text{BEND}} | J K''=K' \gamma''=\gamma' \rangle = \varepsilon h^{\text{BEND}} (-1)^{K'} \cos(2K'\varphi^{\text{BEND}})$$

with $\varepsilon=+1$ (resp. $\varepsilon=-1$) for $\Gamma(\varphi_{\text{vib-tors-bend-rot}})=B_1$ or B_2 (resp. $\Gamma(\varphi_{\text{vib-tors-bend-rot}})=A_1$ or A_2)

$$\langle JK'\gamma' | H^{\text{BEND}} | J K'' \gamma'' \rangle = 0 ; \quad \langle JK'\gamma' | H^{\text{TORS}} | J K'' \gamma'' \rangle = 0$$

if $K' \neq K''$ or $\gamma' \neq \gamma''$.

16/04/2007

36

v- off- diagonal operators

B: B-type Coriolis:

$${}^{v',v}B = {}^{v',v}B_x J_x + {}^{v',v}B_{yz} \{iJ_y, J_z\} + {}^{v',v}B_{xJ} J_x J^2 + {}^{v',v}B_{xzz} \{J_z^2, J_x\} + {}^{v',v}B_{x3} (J_+^3 + J_-^3)$$

C: C-type Coriolis: ${}^{v',v}C = {}^{v',v}C_y iJ_y + {}^{v',v}C_{xz} \{J_x, J_z\}$

Anh: anharmonic operator ${}^{v',v}Anh = {}^{v',v}Anh_{xy} J_{xy}^2 + {}^{v',v}Anh_{xyzz} \{J_z^2, J_{xy}^2\}$

with:

c.c. complex conjugate;

$$\{A, B\} = AB + BA, \quad J_{xy}^2 = J_x^2 - J_y^2, \quad J_{\pm} = J_x \mp iJ_y$$

Wang type functions

$$|JK \gamma\rangle = \frac{1}{\sqrt{2}} (|JK\rangle + \gamma |J-K\rangle) \quad (\text{for } K \neq 0, \gamma = \pm 1) \quad \text{and} \quad |JK = 0 \gamma = +1\rangle = |J0\rangle \quad (\text{for } K=0).$$

Table 7

Hamiltonian constants (in cm^{-1}) for the $\{9^2, 6^1 9^1\}$ polyad of $^{10}\text{BF}_2\text{OH}$

(a) Vibrational energies, rotational, large amplitude torsional parameters

	G.S. ^a	g^2	$6^1 9^1$
φ^{TORS} (in $^\circ$)		1.0933(580)	
$h^{\text{TORS}} \times 10^3$		2.5321(500)	
E_v		1043.88608(8)	1000.5546(650)
$h_{xz}^v \times 10^3$	0.	-3.78530(600)	-3.78530
B_z	0.3442138510	0.34169714(1900)	0.3397651(2800)
B_x	0.3368401260	0.33909619(1900)	0.3371721(2600)
B_y	0.1699352790	0.170013475(180)	0.16960468(5400)
$\Delta_K \times 10^6$	0.361050	0.26634(330)	b
$\Delta_{JK} \times 10^6$	-0.123810	0.06767(300)	b
$\Delta_J \times 10^6$	0.208660	0.168630(140)	-0.2047(170)
$\delta_K \times 10^6$	0.1730980	0.13020(140)	b
$\delta_J \times 10^7$	0.918320	0.718751(780)	b
$H_K \times 10^{11}$	0.2545	b	b
$H_{KJ} \times 10^{11}$	-0.10374	b	b
$H_{JK} \times 10^{12}$	-0.6990	b	b
$H_J \times 10^{12}$	0.5337	b	b
$h_K \times 10^{11}$	0.25600	b	b
$h_{JK} \times 10^{12}$	0.2902	b	b
$h_J \times 10^{12}$	0.2795	b	b

(b) Interaction constant (B- type Coriolis) : ${}^{69,99}B_x = 1.7857(140) \times 10^{-3}$

Table 8Hamiltonian constants (in cm^{-1}) for the $\{9^2, 6^1 9^1\}$ polyad of $^{11}\text{BF}_2\text{OH}$

(a) Vibrational energies, rotational, large amplitude torsional parameters

	G.S. ^a	9^2	$6^1 9^1$
φ^{TORS} (in $^\circ$)		1.2136(390)	
$h^{\text{TORS}} \times 10^3$		2.54516(1000)	
E_V		1042.87549(1)	1001.6994(90)
$h_{XZ}^V \times 10^3$	0.	-3.81573(550)	-3.81573
B_z	0.3442527674	0.34177105(1700)	0.34048063(4300)
B_x	0.3368801619	0.33912576(1700)	0.33753430(6900)
B_y	0.1699552162	0.170036435(160)	0.16971814(1900)
$\Delta_K \times 10^6$	0.360006	0.279582(990)	b
$\Delta_{JK} \times 10^6$	-0.123285	0.05201(100)	b
$\Delta_J \times 10^6$	0.208611	0.170484(400)	-0.08018(740)
$\delta_K \times 10^6$	0.1732762	0.138954(960)	b
$\delta_J \times 10^7$	0.918552	0.72798(190)	b
$H_K \times 10^{11}$	0.2595	b	b
$H_{KJ} \times 10^{11}$	-0.1121	b	b
$H_{JK} \times 10^{12}$	-0.6838	b	b
$H_J \times 10^{12}$	0.5003	b	b
$h_K \times 10^{11}$	0.24951	b	b
$h_{JK} \times 10^{12}$	0.3035	b	b
$h_J \times 10^{12}$	0.2782	b	b

(b) Interaction constant (B-type Coriolis) : $^{69,99}B_x = 1.60934(770) \times 10^{-3}$

Table 9

Hamiltonian constants (in cm^{-1}) for the $\{4^1, 7^1 9^1, 6^1 7^1, \}$ polyad of $^{10}\text{BF}_2\text{OH}$

(a) Vibrational energies, rotational, large amplitude bending parameters

	4^1	$7^1 9^1$	$6^1 7^1$
φ^{BEND} (in $^\circ$)	1.07425(190)		
$h^{\text{BEND}} \times 10^3$	1.78523(100)		
E_v	961.73359(1)	972.80547(4)	932.0071(1)
$h_{xz}^v \times 10^3$	-1.81396(130)	-1.81396	-1.81396
B_z	0.342819186(670)	0.346918002(730)	0.34421697(920)
B_x	0.337792467(620)	0.334863884(740)	0.33832555(100)
B_y	0.1698203486(63)	0.1680236075(840)	0.1702683793(900)
$\Delta_K \times 10^6$	0.1211745(100)	-0.81833(180)	b
$\Delta_{JK} \times 10^6$	0.0345027(900)	0.67876(160)	b
$\Delta_J \times 10^6$	0.22767587(660)	0.115517(190)	b
$\delta_K \times 10^6$	0.3007202(450)	0.429436(530)	b
$\delta_J \times 10^7$	0.9897934(900)	0.796839(920)	b
$H_K \times 10^{11}$	b	b	b
$H_{KJ} \times 10^{11}$	b	b	b
$H_{JK} \times 10^{12}$	b	b	b
$H_J \times 10^{12}$	-0.013268(760)	b	b
$h_K \times 10^{11}$	b	b	b
$h_{JK} \times 10^{12}$	b	b	b
$h_J \times 10^{12}$	b	b	b

(b) Interaction constants

$7^1 9^1 \leftrightarrow 4^1$	B- Coriolis	${}^{79,4}B_x$	$-1.4277277(770) \times 10^{-1}$
		${}^{79,4}B_{xJ}$	$6.02342(160) \times 10^{-6}$
		${}^{79,4}B_{x3}$	$4.83401(140) \times 10^{-6}$
$6^1 7^1 \leftrightarrow 4^1$	C- Coriolis	${}^{67,4}C_{xz}$	$-2.94749(380) \times 10^{-4}$
	Anharmonic	${}^{67,4}A_{xy}$	$5.20874(520) \times 10^{-4}$
		${}^{67,4}A_{xyzz}$	$9.72892(150) \times 10^{-8}$

For Peer Review Only

Table 10

Hamiltonian constants (in cm^{-1}) for the $\{4^1, 7^1 9^1, 6^1 7^1\}$ polyad of $^{11}\text{BF}_2\text{OH}$

(a) Vibrational energies, rotational, large amplitude bending parameters

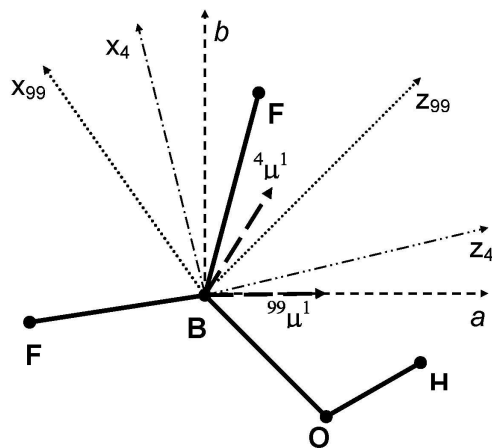
	4^1	$7^1 9^1$	$6^1 7^1$
φ^{BEND} (in $^\circ$)	1.20244(250)		
$h^{\text{BEND}} \times 10^3$	1.89810(160)		
E_V	961.49330(1)	970.99570(1)	929.2077(6)
$h_{XZ}^V \times 10^3$	-1.44363(170)	-1.44363	-1.44363
B_Z	0.342982214(660)	0.343420051(900)	0.37616993(430)
B_X	0.338127986(660)	0.337759784(900)	0.32158867(190)
B_Y	0.1698268850(70)	0.1680406191(440)	0.172324425(360)
$\Delta_K \times 10^6$	0.462518(110)	0.284814(370)	-3.01463(270)
$\Delta_{JK} \times 10^6$	-0.3377696(860)	-0.104067(380)	4.41391(200)
$\Delta_J \times 10^6$	0.25790756(26)	0.1859195(990)	0.238714(530)
$\delta_K \times 10^6$	0.1719722(840)	b	b
$\delta_J \times 10^7$	0.919588(160)	1.362515(510)	-4.85529(260)
$H_K \times 10^{11}$	b	b	b
$H_{KJ} \times 10^{11}$	b	b	b
$H_{JK} \times 10^{12}$	b	b	b
$H_J \times 10^{12}$	b	b	b
$h_K \times 10^{11}$	b	b	b
$h_{JK} \times 10^{12}$	b	b	b
$h_J \times 10^{12}$	b	b	b

(b) Interaction constants

$7^1 9^1 \leftrightarrow 4^1$	B- Coriolis	${}^{79,4}B_x$	$-1.5583049(210) \times 10^{-1}$
		${}^{79,4}B_{xJ}$	$-2.82945(380) \times 10^{-6}$
		${}^{79,4}B_{xzz}$	$4.77886(610) \times 10^{-6}$
		${}^{79,4}B_{x3}$	$3.59167(280) \times 10^{-7}$
$6^1 7^1 \leftrightarrow 4^1$	Anharmonic	${}^{67,4}A_{xy}$	$3.76857(220) \times 10^{-4}$
		${}^{67,4}A_{xyzz}$	$-1.03756(130) \times 10^{-7}$

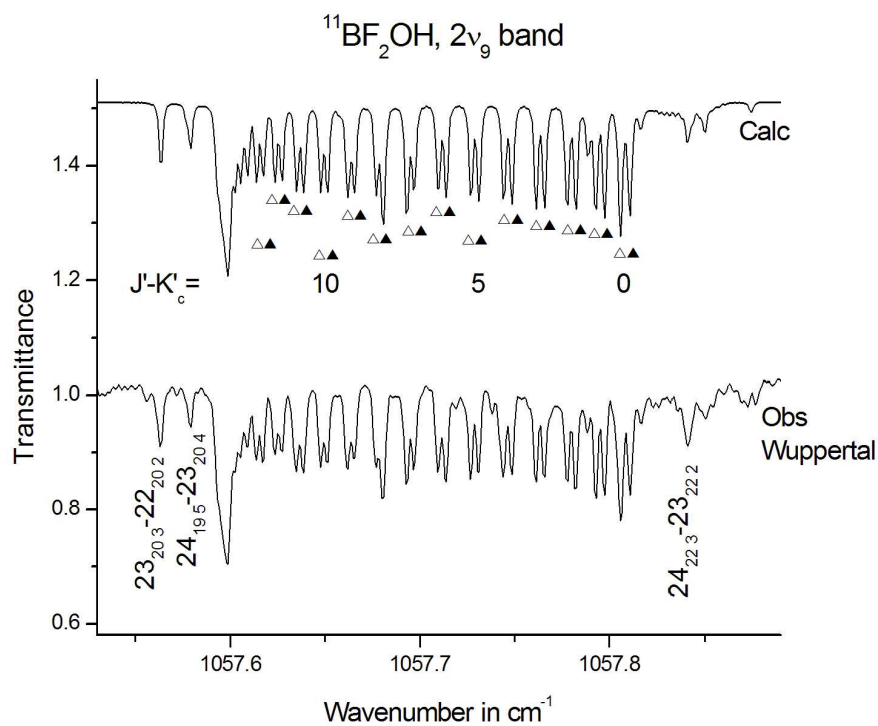
For Peer Review Only

1
2
3
4
5
6
7
8
9
10
11
12
13
14
15
16
17
18
19
20
21
22
23
24
25
26
27
28
29
30
31
32
33
34
35
36
37
38
39
40
41
42
43
44
45
46
47
48
49
50
51
52
53
54
55
56
57
58
59
60

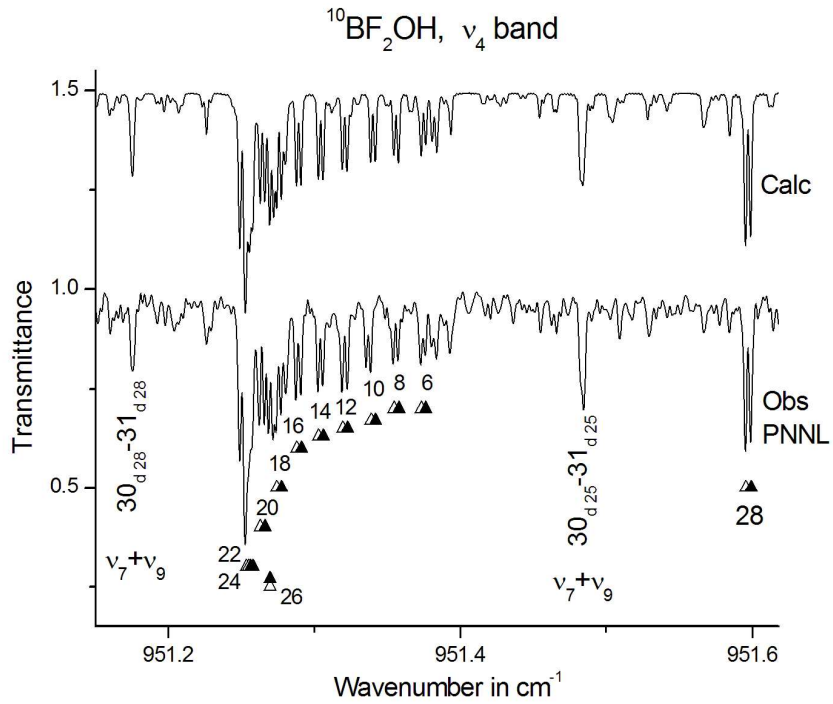


297x209mm (200 x 200 DPI)

view Only

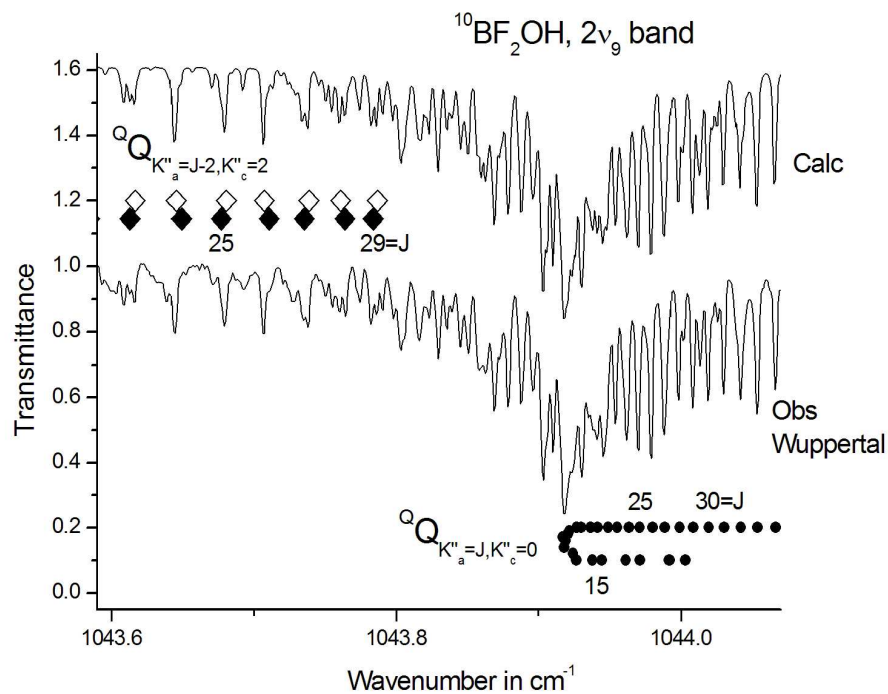


279x215mm (150 x 150 DPI)

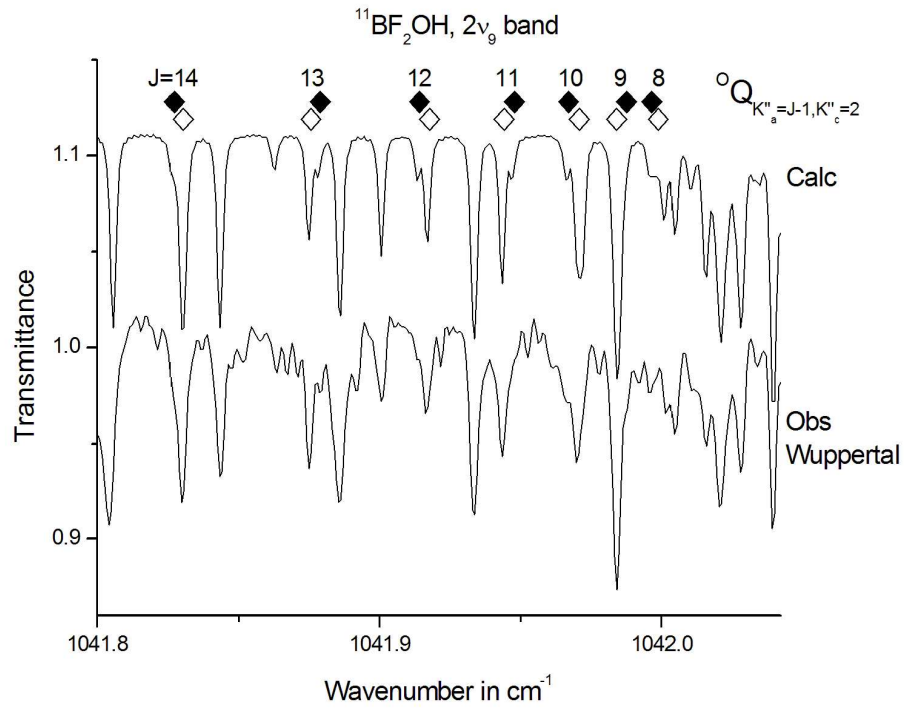


279x215mm (150 x 150 DPI)

View Only



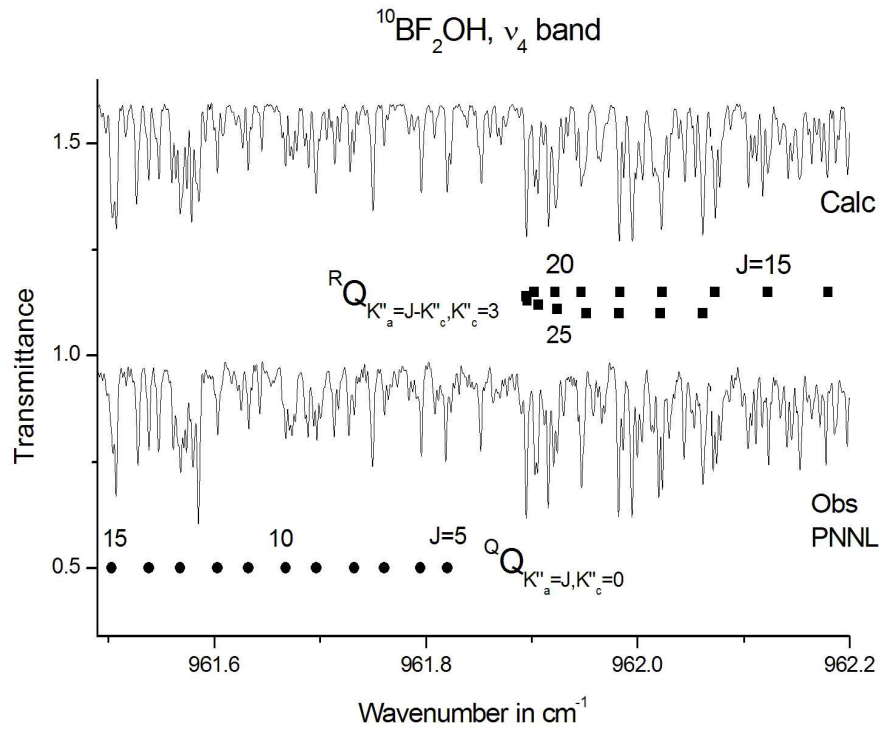
279x215mm (150 x 150 DPI)



279x215mm (150 x 150 DPI)

View Only

1
2
3
4
5
6
7
8
9
10
11
12
13
14
15
16
17
18
19
20
21
22
23
24
25
26
27
28
29
30
31
32
33
34
35
36
37
38
39
40
41
42
43
44
45
46
47
48
49
50
51
52
53
54
55
56
57
58
59
60

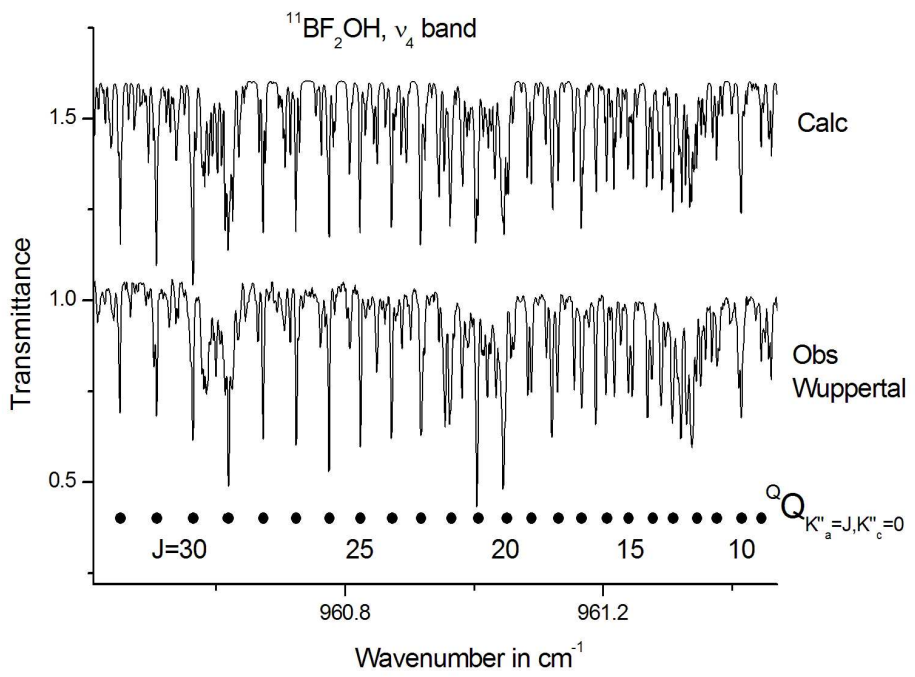


279x215mm (150 x 150 DPI)

NEW Only

URL: <http://mc.manuscriptcentral.com/tandf/tmph>

1
2
3
4
5
6
7
8
9
10
11
12
13
14
15
16
17
18
19
20
21
22
23
24
25
26
27
28
29
30
31
32
33
34
35
36
37
38
39
40
41
42
43
44
45
46
47
48
49
50
51
52
53
54
55
56
57
58
59
60



279x215mm (150 x 150 DPI)

View Only